



Cite this: RSC Adv., 2017, 7, 43403

Received 21st June 2017  
Accepted 30th August 2017DOI: 10.1039/c7ra06906e  
[rsc.li/rsc-advances](http://rsc.li/rsc-advances)

## Highly uniform hierarchical $Zn_2SnO_4$ microspheres for the construction of high performance dye-sensitized solar cells†

Xin Wang,<sup>ab</sup> Yu-Fen Wang,<sup>\*ab</sup> Qiu-Ping Luo,<sup>c</sup> Jian-Hua Ren,<sup>ab</sup> De-Jun Li<sup>ab</sup> and Xi-Fei Li<sup>ID, \*ab</sup>

3D hierarchical  $Zn_2SnO_4$  microspheres show great potential as alternative photoanodes for dye-sensitized solar cells (DSSCs). Herein, hierarchical  $Zn_2SnO_4$  microspheres with different sizes are fabricated *via* a one-step hydrothermal method, and a plausible formation process for  $Zn_2SnO_4$  microspheres is proposed. The DSSCs devices based on 1.20  $\mu\text{m}$   $Zn_2SnO_4$  microspheres show the best power conversion efficiency (PCE) of 4.00%. Further,  $TiCl_4$  treatment of a  $Zn_2SnO_4$  microsphere photoanode results in an improved PCE up to 4.72%.

### 1. Introduction

Since the pioneering report of dye-sensitized solar cells (DSSCs) by M. Grätzel in 1991, tremendous progress has been witnessed in this field over the past decades.<sup>1,2</sup> So far, the highest power conversion efficiencies (PCEs) of more than 14% have been demonstrated.<sup>3</sup> The photoanodes, composed of wide-band-gap semiconducting metal oxide films (such as  $TiO_2$ ,  $ZnO$ ,  $SnO_2$  and  $Zn_2SnO_4$ ) with a large internal surface area, play a key role in affecting the photovoltaic performance of DSSCs.<sup>4–11</sup> Ternary oxide semiconductors, such as  $Zn_2SnO_4$ , have attracted worldwide attention due to their promising optical and electrical properties. Firstly,  $Zn_2SnO_4$  possesses a wide band gap of 3.8 eV ( $TiO_2$ : 3.2 eV), whose conduction band position is similar to that of  $TiO_2$  and  $ZnO$ . However, for these two metal oxides,  $TiO_2$  and  $ZnO$ , the UV region of the solar spectrum suffers from photo-bleaching when applied as photoanodes in DSSCs;<sup>12</sup> secondly,  $Zn_2SnO_4$  with a higher electron mobility of 10–15  $\text{cm}^2 \text{V}^{-1} \text{s}^{-1}$  than  $TiO_2$  (10–5  $\text{cm}^2 \text{V}^{-1} \text{s}^{-1}$ ) implies more efficient electron transport characteristic in DSSCs.<sup>13,14</sup> Thirdly, unlike  $ZnO$ , for which the Zn-dye + complex can decrease the photocurrent ( $J_{sc}$ ) and photovoltage ( $V_{oc}$ ),  $Zn_2SnO_4$  shows better chemical stability in acid/based solution.<sup>15</sup> Last but not least,  $Zn_2SnO_4$  possesses tunable work function and electric resistivity. It is well-known that the hierarchical structured materials have several

advantages while are applied in DSSCs, for instance, the large specific surface area could induce efficient dye adsorption, outstanding light-scattering ability could induce efficient light harvesting, and well-interconnected structures could induce boosted electron transport and suppressed electron recombination.<sup>16–18</sup> But, fabrication of  $Zn_2SnO_4$  microspheres with uniform morphological features pose the greatest challenge in their preparation because such ternary oxide needs high temperature (>200 °C) to crystallize and regulate the Zn and Sn ions during synthetic process.

In this work, we demonstrate a facile one-step hydrothermal process to fabricate 3D hierarchically  $Zn_2SnO_4$  microspheres consisting of nanoplates, which could offer not only larger surface areas but also would result in a better light-scattering ability as well as electricity-generation properties. In addition,  $TiO_2$ -coated hierarchical  $Zn_2SnO_4$  microspheres (~1.2  $\mu\text{m}$  in diameter) are used as photoanode materials for improved PCE in DSSCs. The highest PCE in this work up to 4.72% has been achieved.

### 2. Experimental

#### 2.1 Synthesis

Hierarchical  $Zn_2SnO_4$  microspheres are synthesized *via* a one-step hydrothermal process. Typically, 1.402 g  $SnCl_4 \cdot 5H_2O$  (A.R.), 1.756 g  $Zn(CH_3COO)_2 \cdot 2H_2O$  (A.R.), 1.776 g  $NH_4F$  (A.R.), 1.480 g  $H_3BO_3$  (A.R.) are dissolved in 80 mL distilled  $H_2O$  in a 100 mL Teflon-lined container. Then, 2.0 g  $NaOH$  is added into the above solution with vigorous stirring. After continuously stirring for another 30 min, the obtained precursor solution is transferred to a stainless steel autoclave. After being sealed, the autoclave is kept heated at 200 °C for 24 h. While being cooled to the room temperature, the obtained solution is purified by centrifuging using 6000 rpm for 5 min to get the

<sup>a</sup>Energy & Materials Engineering Center, College of Physics and Materials Science, Tianjin Normal University, Tianjin 300387, China. E-mail: xfli@mail.tjnu.edu.cn; yfwang@mail.tjnu.edu.cn

<sup>b</sup>Tianjin International Joint Research Center of Surface Technology for Energy Storage Materials, Tianjin 300387, China

<sup>c</sup>Laboratory of Optical Information Technology, School of Science, Wuhan Institute of Technology, Wuhan 430205, China

† Electronic supplementary information (ESI) available. See DOI: 10.1039/c7ra06906e

precipitates. During the centrifuge process, the precipitates are washed 3 times with absolute ethanol and distilled water in an ultrasonic cleaning bath for 10 min, respectively. The final white-color power is dried at 70 °C for the further characterizations. In order to tune the diameter of the hierarchical  $Zn_2SnO_4$  microspheres, diethylene glycol (DEG) and ethylene glycol (EG) are used as the mixed solvent to support the  $Zn_2SnO_4$  crystal growth.

## 2.2 Preparation of the $Zn_2SnO_4$ microspheres photoanode

First, the FTO glass (sheet resistance: 15 Ω/square, Nippon Sheet Glass, Japan) is ultrasonically cleaned with water, HCl (A.R.), acetone (A.R.) and ethanol (A.R.) for 30 min, successively. 1.0 g hierarchical  $Zn_2SnO_4$  samples are ground for 30 min in the mixtures (8.0 mL ethanol, 3.0 g terpineol, 0.2 mL acetic acid and 0.5 g ethyl cellulose) to form slurry, and then the obtained mixtures are sonicated in an ultrasonic bath for 15 min, finally to form  $Zn_2SnO_4$  paste. The preparation of  $Zn_2SnO_4$  paste is the same to the previous report. The obtained different  $Zn_2SnO_4$  paste is coated on the cleaned FTO glass *via* the screen-printing technique. Meanwhile, the thickness of  $Zn_2SnO_4$  film is adjusted through repeating the screen-printing times. Then, the obtained different  $Zn_2SnO_4$  films are heated at 500 °C for 1.0 h in air. After that, the obtained different  $Zn_2SnO_4$  films are immersed into a 40 mM  $TiCl_4$  aqueous solution for another 30 min at 70 °C, followed by annealing at 520 °C for 30 min. When cooling down to room temperature, the fabricated  $Zn_2SnO_4$  photoanodes are soaked into N719 dye solution (Ru [LL'-NCS]<sub>2</sub>, L = 2,2'-bipyridyl-4,4'-dicarboxylic acid, L = 2,2'-bipyridyl-4,4'-ditetrabutylammonium carboxylate, 5.0 × 10<sup>-4</sup> M, Solaronix Co.) in acetonitrile/tert-butanol (1 : 1, v/v) for 24 h. The Pt counter electrode is prepared *via* adding  $H_2PtCl_6$  solution (5.0 × 10<sup>-4</sup> M) on the surface of the cleaned FTO glass, and then heat at 400 °C for 15 min in air. And the electrolyte is consisted of  $I_2$  (0.03 M), 1-propyl-3-methyl-imidazolium iodide (PMII, 0.6 M), LiI (0.05 M), guanidine thiocyanate (GuNCS, 0.1 M, Aldrich), and 4-*tert*-butylpyridine (*t*-BP, 0.5 M, Aldrich) in a mixture contained acetonitrile and valeronitrile (85 : 15, v/v). And the active area of the N719 dye-sensitized  $Zn_2SnO_4$  films in this work is about 0.152 cm<sup>2</sup>.

## 2.3 Characterization

The phase purity of the products is characterized by powder X-ray diffraction (XRD) (Bruker D8 Advance X-ray diffractometer, Cu K $\alpha$  radiation,  $\lambda$  = 1.5418 Å). The morphology is investigated by field emission scanning electron microscopy (FE-SEM, SU8010) and transmission electron microscope (TEM, JEOL-2010). And the thickness of  $Zn_2SnO_4$  film is determined *via* a profilometer (Ambios, XP-2). UV-vis diffused reflectance spectra is investigated on a UV-vis-NIR Spectrophotometer (Shimadzu UV-3600). The current-voltage (*J*-*V*) characteristics in this work are performed with Keithley 2400 source meter, (AM 1.5 G illumination, 100 mW cm<sup>-2</sup>), which are provided by solar simulator (69 920, 1 kW Xe lamp, Oriel). The standard Si solar cell with different optical filter (Oriel) provides various irradiance intensities (from 0.1 to 1.0 sun), is introduced to calibrate the

incident light intensity. Incident photon-to-current conversion efficiency (IPCE) signal is recorded on a Keithley 2000 multimeter under the illumination of a 150 W tungsten lamp with a Spectral Product DK240 monochromator. The intensity-modulated photovoltage spectroscopy (IMVS) and intensity-modulated photocurrent spectroscopy (IMPS) measurements (two electrode polarization scheme) are carried on an electrochemical workstation (Zahner, Zennium), under the modulated blue light emitting diodes (457 nm) driven by a Zahner (PP211) source supply, the electrochemical workstation with a frequency-response analyzer. The electrochemical impedance spectroscopy (EIS) is also performed on an electrochemical workstation (Zahner, Zennium) in dark (bias potential: -0.70 V, frequency range: 10 mHz to 1 MHz).

## 3. Results and discussion

In this study,  $Zn(CH_3COO)_2 \cdot 2H_2O$  and  $SnCl_4 \cdot 5H_2O$  are used as precursors in the hydrothermal process. The phase structures of prepared samples are characterized by XRD. As shown in Fig. 1a, all peaks are well consistent with pure cubic structure of  $Zn_2SnO_4$  with the lattice constants of  $a = b = c = 8.657$  Å (JCPDS No. 24-1470). And the strong signal of characteristic peaks indicates the high crystallinity of as-prepared  $Zn_2SnO_4$  microspheres. As seen in Fig. 1b, the obtained  $Zn_2SnO_4$  microspheres have a uniform size distribution with diameter of 1.20 μm. Fig. 1c shows the hierarchical structure of as-prepared  $Zn_2SnO_4$  microsphere with a relatively rough surface. Specifically, the microsphere composes of numerous cross-linked and interconnected nanosheets. Fig. 1d confirms the microscale of the  $Zn_2SnO_4$  spheres.

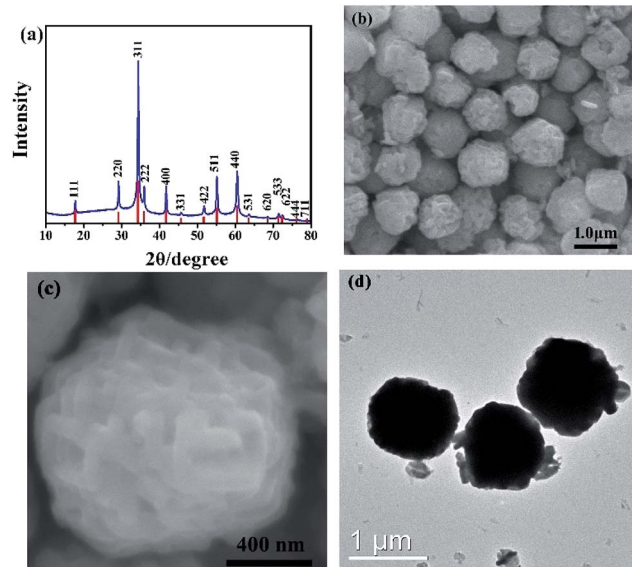


Fig. 1 (a) XRD patterns of as-synthesized  $Zn_2SnO_4$  microspheres after hydrothermal reaction for 24 h. (b) Low-magnification and (c) high-magnification FE-SEM images of as-prepared  $Zn_2SnO_4$  microsphere. (d) TEM image of  $Zn_2SnO_4$  microspheres.

The time-dependent experiments are carried out to explore the detail formation process of the hierarchical  $Zn_2SnO_4$  microspheres. As shown in Fig. 2, the morphologies of the  $Zn_2SnO_4$  are delicately dependent on the hydrothermal reaction time. An interesting morphological evolution has been observed (Fig. 2, 1b and c) since reaction time increased from 1 h to 24 h. At the early stage (1 h), the  $Zn_2SnO_4$  nanoplates are observed (Fig. 2a). Increasing the time to 2 h, the primary nanoplates occur to connect with each other to form a cross-shaped  $Zn_2SnO_4$  structure (Fig. 2b). Prolonging the hydrothermal reaction time to 4 h, one can observe the formation of the irregular  $Zn_2SnO_4$  hemispheres ( $\sim 0.6\ \mu m$  in diameter), which consist of numerous interconnected nanosheets (Fig. 2c). The semi-matured hierarchical  $Zn_2SnO_4$  microspheres ( $\sim 1.0\ \mu m$  in diameter) can be obtained when the hydrothermal reaction increases to 12 h, as shown in Fig. 2d. Further increasing the hydrothermal time to 24 h leads to the formation of well-defined hierarchical  $Zn_2SnO_4$  microspheres ( $\sim 1.20\ \mu m$  in diameter) which are made up of cross-linked and interconnected nanosheets (Fig. 1b and c).

Based on the above discussion, a possible growth process of the hierarchical  $Zn_2SnO_4$  microspheres is proposed (Scheme 1). During the initial stage, the Zn and Sn precursor results in the self-assembly formation of primary  $Zn_2SnO_4$  nanoplates, and then the cross-shaped  $Zn_2SnO_4$  structure is formed *via* the interconnection between nanoplates. With further aggregation of these  $Zn_2SnO_4$  nanoplates, an irregular  $Zn_2SnO_4$  hemisphere is formed. Gradually, the newly formed nanoplates selectively attach onto the surface of existing secondary structure, which evolves to the final 3D hierarchical  $Zn_2SnO_4$  microspheres *via* the self-assemble process.

The preliminary study proved the diethylene glycol (DEG) can influence the sizes of the samples.<sup>8</sup> Hence, in order to tune the diameter of the hierarchical  $Zn_2SnO_4$  microspheres, DEG and EG are used as the mixed solvent to support the  $Zn_2SnO_4$

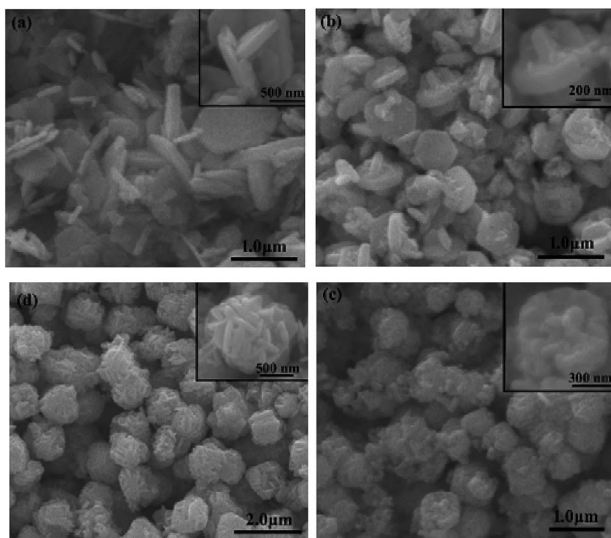
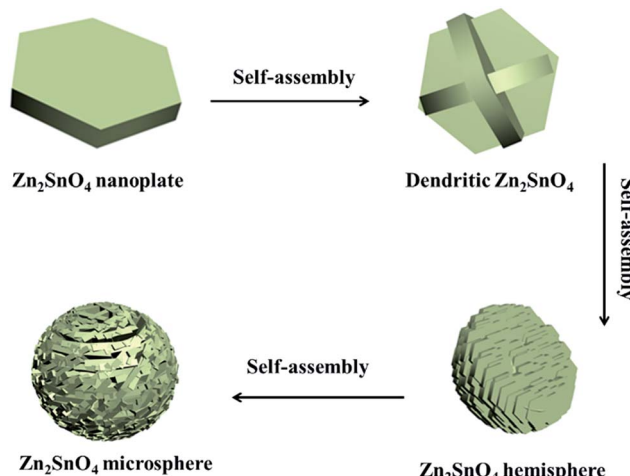


Fig. 2 FE-SEM images of the  $Zn_2SnO_4$  microspheres synthesized at different hydrothermal time: (a) 1 h, (b) 2 h, (c) 4 h, (d) 12 h. The inset images are the corresponding high-magnification FE-SEM images.



Scheme 1 Schematic illustration of the formation process of the as-prepared hierarchical  $Zn_2SnO_4$  microspheres.

crystal growth. Meanwhile, it is found that the composition of solvent significantly affects the sizes of  $Zn_2SnO_4$  microspheres. The FE-SEM and TEM images of the  $Zn_2SnO_4$  spheres prepared under the different solvent conditions, as shown in Fig. 3. Typically, EG/ $H_2O$  (20 : 60 in volume ratio) and DEG/ $H_2O$  (20 : 60 in volume ratio) lead to the formation of hierarchical  $Zn_2SnO_4$  microspheres with average size of 0.85  $\mu m$  and 0.60  $\mu m$ , respectively, which are smaller than that of pure  $H_2O$ -based counterpart (1.20  $\mu m$ ). According to the previous investigation results, the growth rates of crystals vary along the different crystallographic directions, so that the final morphology is controlled by the fastest growth plane.<sup>19</sup> The influences of EG

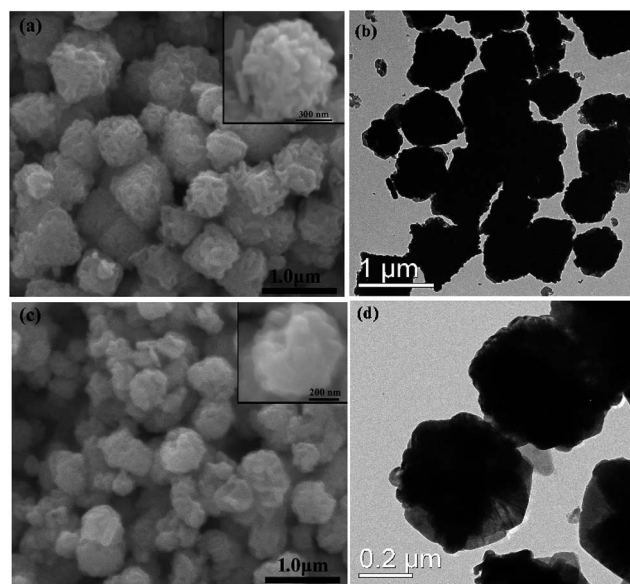


Fig. 3 FE-SEM and TEM images of  $Zn_2SnO_4$  microspheres prepared with  $V_{EG} : V_{H_2O} = 20 : 60$  (a and b) and  $V_{DEG} : V_{H_2O} = 20 : 60$  (c and d), respectively, in the meantime, other experimental conditions are kept constant. Insets in (b) and (d) are the corresponding high-magnification FE-SEM images.

and DEG on the sizes of hierarchical  $Zn_2SnO_4$  microspheres may be attributed to their coordination ability with initial Zn and Sn precursor as well as their reactivity, which can alter the  $Zn_2SnO_4$  nuclei and growth rates on the different crystal planes, in other words, leading to different size  $Zn_2SnO_4$  microspheres. However, further work need to be carried out to studied how EG and DEG exactly effect on the sizes of  $Zn_2SnO_4$  microspheres.

The hierarchical  $Zn_2SnO_4$  microsphere photoanodes are prepared by screen-printing procedures according to our previous report.<sup>12</sup> The photovoltaic properties of DSSCs based on three different sizes hierarchical  $Zn_2SnO_4$  microspheres are tested by recording the  $J$ - $V$  characteristics under AM 1.5 G illumination (100 mW  $cm^{-2}$ ) conditions. The  $J$ - $V$  curves are shown in Fig. 4a and the detailed photovoltaic parameters ( $J_{sc}$ ,  $V_{oc}$ , PCEs and FF) are summarized in Table 1. The DSSC with 0.60  $\mu m$  hierarchical  $Zn_2SnO_4$  microspheres shows the lowest PCE of 2.91% with a  $J_{sc}$  of 6.17  $mA\ cm^{-2}$ , a  $V_{oc}$  of 661 mV and a FF of 0.71. By contrast, the devices based on 0.85  $\mu m$  hierarchical  $Zn_2SnO_4$  microspheres shows slightly improved photovoltaic performances with a  $J_{sc}$  of 7.21  $mA\ cm^{-2}$ , a  $V_{oc}$  of 691 mV, a FF of 0.71 and a PCE of 3.56%. The cells based on 1.20  $\mu m$  hierarchical  $Zn_2SnO_4$  microspheres shows the best photovoltaic performance with improved  $J_{sc}$  (7.82  $mA\ cm^{-2}$ ),  $V_{oc}$  (716 mV) and FF (0.71), leading to an enhanced PCE up to 4.00%. One can see a clear tendency that the  $J_{sc}$  improves with increasing sizes of the hierarchical  $Zn_2SnO_4$  microspheres. The dark  $J$ - $V$  characteristics in Fig. 4 also reveal that the dark photocurrents increase in the order of 1.20  $\mu m$   $Zn_2SnO_4$  microspheres < 0.85  $\mu m$   $Zn_2SnO_4$  microspheres < 0.60  $\mu m$   $Zn_2SnO_4$  microspheres, indicating the suppressed charge recombination along with increased sizes of the hierarchical  $Zn_2SnO_4$  microspheres.

The incident photon-to-current efficiency (IPCE), defined as the number of electrons generated by light in the external circuit divided by the number of incident photons, is plotted as

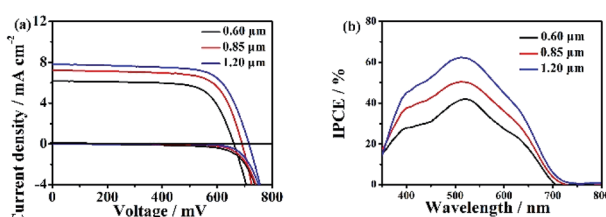


Fig. 4 (a) Photocurrent density–voltage ( $J$ – $V$ ) curves and (b) incident photon-to-current (IPCE) curves of the DSSCs devices based on different sizes  $Zn_2SnO_4$  photoanodes with the film thickness of  $\sim 15\ \mu m$ .

Table 1 Detailed photovoltaic parameters ( $J_{sc}$ ,  $V_{oc}$ , PCE and FF) of DSSCs with different  $Zn_2SnO_4$  photoanodes

DSSCs	$J_{sc}/mA\ cm^{-2}$	$V_{oc}/mV$	$\eta/\%$	FF	Adsorbed dye/ $10^{-8}\ mol\ cm^{-2}$
0.60 $\mu m$	6.17	661	2.91	0.71	20.16
0.85 $\mu m$	7.21	691	3.56	0.71	19.87
1.20 $\mu m$	7.82	716	4.00	0.71	18.62

a function of excitation wavelength, which shows the maximal value at 530 nm increase with the increasing microspheres size (Fig. 4b), which is consistent with the  $J_{sc}$  and  $\eta$ .

The loading amount of N719 dye decreases with increasing sizes of the hierarchical  $Zn_2SnO_4$  microspheres due to the decreased surface area of the larger microspheres. In addition to the N719 dye loading amount, as well known that, the light scattering ability of the  $Zn_2SnO_4$  photoanodes can also influence the light utilization capability through altering the path and/or extending the distance of light travelled, and in this way, the light-harvesting efficiency is improved, which would lead to an enhancement of the  $J_{sc}$  and thus PCE.

The light scattering ability of three different sizes of the hierarchical  $Zn_2SnO_4$  microspheres films is determined by diffused reflectance spectroscopy, as shown in Fig. 5. For the larger-sized hierarchical  $Zn_2SnO_4$  microspheres, the reflectance increases in the whole visible range (500–800 nm), indicating stronger light scattering ability which could maximize the utilization of incident light, thus enhancing the light harvesting efficiency and  $J_{sc}$ . Accordingly, the 1.20  $\mu m$   $Zn_2SnO_4$  microspheres exhibits the best light scattering capability, which is in good agreement with its highest  $J_{sc}$  (7.82  $mA\ cm^{-2}$ ).

In Fig. 6, the IMPS and IMVS are performed to determine the electron transport and recombination characteristics of the devices based on the three different  $Zn_2SnO_4$  photoanodes. The detailed parameters extracted from IMPS and IMVS measurements are summarized in Table 2 (light intensity: 150  $W\ m^{-2}$ ). The electron transport time ( $\tau_d$ ) or recombination time ( $\tau_r$ ) is obtained from the expression  $\tau_d = 1/2\pi f_d$  or  $\tau_r = 1/2\pi f_r$ , respectively, where  $f_d$  or  $f_r$  is the characteristic frequency minimum of the IMPS/IMVS imaginary component. The  $\tau_d$  and  $\tau_r$  (Fig. 6a) decreases with increasing light intensity because the deep traps are filled by the more photo-electrons generated at higher light intensity, resulting in electron trapping/detrapping involved shallower levels.<sup>20</sup> As summarized in Table 2, the 1.20  $\mu m$   $Zn_2SnO_4$  microspheres exhibits the shorter electron transport time (1.17 ms) than the 0.85  $\mu m$   $Zn_2SnO_4$  microspheres (1.88 ms) and the 0.60  $\mu m$   $Zn_2SnO_4$  microspheres (2.25 ms), implying that the 1.20  $\mu m$   $Zn_2SnO_4$  microsphere is more efficient in terms of electron transport than smaller sized  $Zn_2SnO_4$  microspheres. In contrast, the electron lifetime of the 1.20  $\mu m$   $Zn_2SnO_4$  microspheres (27.76 ms) is longer than the 0.85  $\mu m$   $Zn_2SnO_4$  microspheres (15.67 ms) and the 0.60  $\mu m$   $Zn_2SnO_4$

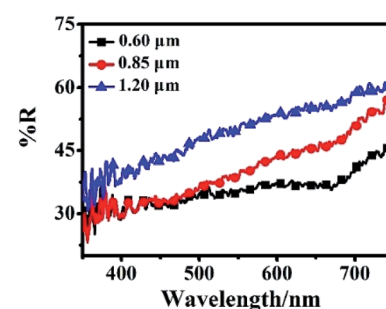


Fig. 5 Diffused reflectance spectra of different  $Zn_2SnO_4$  films without N719 dye.

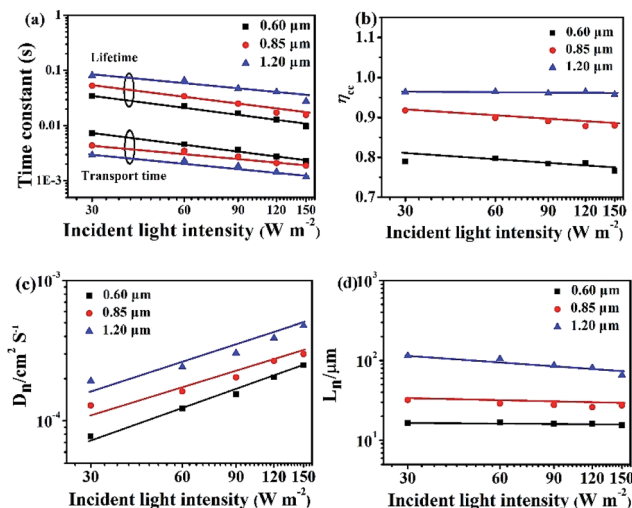


Fig. 6 (a) Light intensity dependent electron transport time and lifetime, (b) electron collection efficiency, (c) electron diffusion coefficient and (d) effective electron diffusion length of the DSSCs based on different Zn<sub>2</sub>SnO<sub>4</sub> photoanodes with the film thickness of ~15.0 μm.

Table 2 Detailed parameters ( $\tau_d$ ,  $\tau_r$ ,  $\eta_{cc}$ ,  $D_n$ , and  $L_n$ ) extracted from IMPS and IMVS measurements for DSSCs based on different Zn<sub>2</sub>SnO<sub>4</sub> photoanodes with a film thickness of ~15.0 μm. Light intensity: 150 W m<sup>-2</sup>

DSSCs	$\tau_d$ (ms)	$\tau_r$ (ms)	$\eta_{cc}$ /%	$D_n$ (cm <sup>2</sup> s <sup>-1</sup> )	$L_n$ (μm)
1.20 μm	1.17	27.76	95.8	$4.79 \times 10^{-4}$	65.6
0.85 μm	1.88	15.67	88.0	$3.00 \times 10^{-4}$	27.3
0.60 μm	2.25	9.63	76.6	$2.49 \times 10^{-4}$	15.5

microspheres (9.63 ms), indicating much more suppressed charge recombination within larger sized microspheres-based devices than the small microspheres-based counterpart, thus leading to enhanced  $V_{oc}$  (716 mV) for the former.

According to the  $\tau_d$  and  $\tau_r$ , one can further acquire another important parameter of the DSSCs, namely, electron collection efficiency ( $\eta_{cc}$ ,  $\eta_{cc} = 1 - \tau_d/\tau_r$ ).<sup>21,22</sup> Fig. 6b shows the  $\eta_{cc}$  of the DSSCs based on three different sized hierarchical Zn<sub>2</sub>SnO<sub>4</sub> photoanodes. It is clear that the  $\eta_{cc}$  of 1.20 μm Zn<sub>2</sub>SnO<sub>4</sub> microspheres-based device (95.8%) is much superior to the 0.85 μm Zn<sub>2</sub>SnO<sub>4</sub> microspheres (88.0%) and 0.60 μm Zn<sub>2</sub>SnO<sub>4</sub> microspheres-based counterparts (76.6%). Herein, the higher  $\eta_{cc}$  also contributes to the higher  $J_{sc}$  for DSSCs based on 1.20 μm Zn<sub>2</sub>SnO<sub>4</sub> microspheres.

Moreover, the effective electron diffusion length ( $L_n$ ) can suggest if the injected electron can transport to external circuit through the photoanode film. At the same time, the  $L_n$  can influence the  $J_{sc}$  and  $\eta$ . The  $L_n$  can be obtained according to the followed equation:  $L_n = (D_n \times \tau_r)/2$ , where  $D_n = d^2/(4 \times \tau_d)$ ,  $D_n$  is the electron diffusion coefficient and  $d$  is the Zn<sub>2</sub>SnO<sub>4</sub> film thickness. As shown in Fig. 6c and Table 2, along with the increasing spherical diameter, the  $D_n$  increases, suggesting that the electron diffusion is faster in Zn<sub>2</sub>SnO<sub>4</sub> microspheres with larger size.

Based on the  $D_n$  (Fig. 6c) and  $\tau_r$  (Fig. 6a),  $L_n$  can be calculated. The DSSCs based on 1.20 μm hierarchical Zn<sub>2</sub>SnO<sub>4</sub> microspheres (65.6 μm) is longer than 0.85 μm hierarchical Zn<sub>2</sub>SnO<sub>4</sub> microspheres (27.3 μm) and 0.60 μm hierarchical Zn<sub>2</sub>SnO<sub>4</sub> microspheres (15.5 μm), implying that the photogenerated electrons can travel through a longer distance within the hierarchical Zn<sub>2</sub>SnO<sub>4</sub> microspheres film (~1.20 μm in diameter), which in turn, guarantees a better charge collection efficiency for such devices.

Based on the discussion above, the enhancement of  $J_{sc}$ ,  $V_{oc}$  and PCE of 1.20 μm hierarchical Zn<sub>2</sub>SnO<sub>4</sub> microspheres-based DSSCs devices due to its superior light scattering, fastest electron transport rates and slowest electron recombination rates.

EIS is a powerful tool to investigate the electrochemical and photoelectrochemical kinetics processes, which can be used to measure the charge transport dynamics of the present DSSCs based on hierarchical Zn<sub>2</sub>SnO<sub>4</sub> microspheres with different sizes. The Nyquist plots of the EIS are shown in Fig. 7. Typically, two semicircles are observed, which can provide good understanding and additional information on the interfacial transfer of photoexcited electrons in the present DSSCs. Generally, the first small semicircle (located in 1 kHz to 1 MHz) corresponds to the charge-transfer resistance at the interface between redox electrolyte/Pt counter electrode. One can see a similar value of resistance because of the utilization of the same electrolyte and counter electrode within the three Zn<sub>2</sub>SnO<sub>4</sub> DSSCs. The second large semicircle (located in 0.1–1 kHz) is attributed to the recombination resistance across the Zn<sub>2</sub>SnO<sub>4</sub>/redox electrolyte interface.<sup>12</sup> It is found that the recombination resistance ( $R_2$ , obtained from Z-view software) increases gradually from 92.3 Ω to 268.6 Ω, when the sizes of hierarchical Zn<sub>2</sub>SnO<sub>4</sub> microsphere size increases from 0.60 μm to 1.20 μm. And the electron lifetime of 1.20 μm Zn<sub>2</sub>SnO<sub>4</sub> microspheres, 0.85 μm Zn<sub>2</sub>SnO<sub>4</sub> microspheres and 0.60 μm Zn<sub>2</sub>SnO<sub>4</sub> microspheres-based devices is 28.12 ms, 15.78 ms and 9.89 ms, respectively. Obviously, 1.20 μm Zn<sub>2</sub>SnO<sub>4</sub> microspheres-based devices exhibit the longest electron lifetime, suggesting that the back reaction (between the injected electrons and the I<sub>3</sub><sup>-</sup> in the electrolyte) is inhibited more effectively. In this case, the highest  $V_{oc}$  is

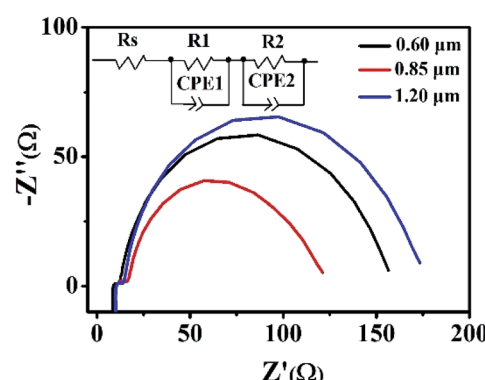


Fig. 7 The impedance spectra (Nyquist plots) of DSSCs based on the three different hierarchical Zn<sub>2</sub>SnO<sub>4</sub> photoanodes with a film thickness of ~15 μm measured at -0.7 V bias in the dark.

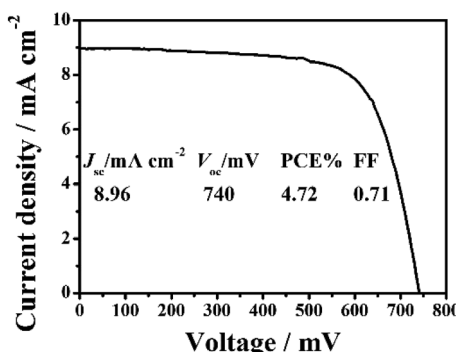


Fig. 8  $J$ - $V$  characteristic of DSSCs based on the  $\sim 15.0$   $\mu\text{m}$  thick hierarchical  $\text{Zn}_2\text{SnO}_4$  microspheres (1.20  $\mu\text{m}$ ) coated with the  $\text{TiO}_2$  shell.

observed. Notably, the electron lifetime variation and tendency obtained from the EIS is consistent with the aforementioned IMVS data as well.

The conduction band (CB) potential of  $\text{TiO}_2$  is negative than  $\text{Zn}_2\text{SnO}_4$ .  $\text{Zn}_2\text{SnO}_4@\text{TiO}_2$  core-shell structure can not only facilitate the electron transfer from  $\text{TiO}_2$  to  $\text{Zn}_2\text{SnO}_4$ , but also can suppress the recombination rates between the photo-injected electrons in the CB of  $\text{Zn}_2\text{SnO}_4$  and  $\text{I}_3^-$  in the electrolyte, leading to improved  $\eta_{cc}$ , and thus further increasing the  $J_{sc}$ ,  $V_{oc}$  and PCE.<sup>10,12</sup> In this study, the coating of  $\text{TiO}_2$  shell on  $\text{Zn}_2\text{SnO}_4$  film is achieved *via* immersing the  $\text{Zn}_2\text{SnO}_4$  films into  $\text{TiCl}_4$  aqueous solution (40 mM) to form the  $\text{Zn}_2\text{SnO}_4@\text{TiO}_2$  core-shell structure (Fig. 8). As for the DSSCs based on  $\text{Zn}_2\text{SnO}_4@\text{TiO}_2$  core-shell structure, the  $J_{sc}$  increases from 7.82 mA cm<sup>-2</sup> to 8.96 mA cm<sup>-2</sup>, and  $V_{oc}$  increases from 716 mV to 740 mV. This results in a 25% improvement of PCE from 4.00% to 4.72%, which can be attributed to the significant reduction of the back reaction of the photoinjected electrons from  $\text{Zn}_2\text{SnO}_4$  microspheres to the redox electrolyte ( $\text{I}_3^-$ ). Another possible reason of the improvement is that defects at the internal surface can be minimized while the  $\text{TiO}_2$  coating on the  $\text{Zn}_2\text{SnO}_4$  microspheres surface, which facilitates the electron transfer from N719 dye molecules to the  $\text{TiO}_2$  and the  $\text{Zn}_2\text{SnO}_4$  microspheres. Meanwhile, the modification of  $\text{TiO}_2$  shell layer could avoid the presence of extra internal trap sites in a poorly constructed junction on  $\text{Zn}_2\text{SnO}_4$  microspheres.<sup>23</sup>

## 4. Conclusions

In summary, a one-step hydrothermal route is demonstrated to the controllable synthesis of 3D hierarchical  $\text{Zn}_2\text{SnO}_4$  microspheres. We proposed a plausible self-assembly formation process of  $\text{Zn}_2\text{SnO}_4$  microspheres based on the time-dependent morphological evolution observations. When applied as photoanodes in DSSCs, the 1.20  $\mu\text{m}$   $\text{Zn}_2\text{SnO}_4$  microspheres show the best photovoltaic performance with a PCE of 4.00%.  $\text{TiCl}_4$  treatment results in the formation of  $\text{Zn}_2\text{SnO}_4@\text{TiO}_2$  core-shell structured photoanode, which further improve the PCE up to 4.72%. The designed 3D hierarchical  $\text{Zn}_2\text{SnO}_4$  microspheres with promising optical and

electrical properties can be extended to other energy-related applications such as in Li-ion battery, photocatalysis and supercapacitor.

## Conflicts of interest

There are no conflicts to declare.

## Acknowledgements

The authors acknowledge the financial supports from the National Natural Science Foundation of China (51502205), Application Development Foundation of Tianjin Normal University (52XK1508), Scientific Research Foundation of Tianjin Normal University (5RL131), and National Training Program of Innovation and Entrepreneurship for Undergraduates in Tianjin of China (201610065012.00) and Academic Innovation Funding of Tianjin Normal University (52XC1404).

## Notes and references

- 1 B. O'Regan and M. Grätzel, *Nature*, 1991, **353**, 737–740.
- 2 M. Grätzel, *Nature*, 2001, **414**, 338–344.
- 3 K. Kakiage, Y. Aoyama, T. Yano, K. Oya, J. Fujisawa and M. Hanaya, *Chem. Commun.*, 2015, **51**, 15894–15897.
- 4 S. Colodrero, A. Mihi, L. Häggman, M. Ocaña, G. Boschloo, A. Hagfeldt and H. Míguez, *Adv. Mater.*, 2009, **21**, 764–770.
- 5 D. H. Chen, F. Z. Huang, Y. B. Cheng and R. A. Caruso, *Adv. Mater.*, 2009, **21**, 2206–2210.
- 6 M. Ye, D. Zheng, M. Lv, C. Chen, C. Lin and Z. Lin, *Adv. Mater.*, 2013, **25**, 3039–3044.
- 7 W. Q. Wu, Y. F. Xu, C. Y. Su and D. B. Kuang, *Energy Environ. Sci.*, 2014, **7**, 644–649.
- 8 Y. F. Wang, K. N. Li, C. L. Liang, Y. F. Hou, C. Y. Su and D. B. Kuang, *J. Mater. Chem.*, 2012, **22**, 21495–21501.
- 9 Z. Dong, X. Lai, J. E. Halpert, N. Yang, L. Yi, J. Zhai, D. Wang, Z. Tang and L. Jiang, *Adv. Mater.*, 2012, **24**, 1046–1049.
- 10 Y. F. Wang, K. N. Li, Y. F. Xu, H. S. Rao, C. Y. Su and D. B. Kuang, *Nanoscale*, 2013, **5**, 5940–5948.
- 11 Z. Li, Y. Zhou, C. Bao, G. Xue, J. Zhang, J. Liu, T. Yu and Z. Zou, *Nanoscale*, 2012, **4**, 3490–3494.
- 12 S. H. Choi, D. Hwang, D. Y. Kim, Y. Kervella, P. Maldivi, S. Y. Jang, R. Demadrille and I. D. Kim, *Adv. Funct. Mater.*, 2013, **23**, 3146–3155.
- 13 T. J. Coutts, D. L. Young, X. Li, W. P. Mulligan and X. J. Wu, *J. Vac. Sci. Technol., A*, 2000, **18**, 2646–2660.
- 14 Q. F. Zhang, C. S. Dandeneau, X. Y. Zhou and G. Z. Cao, *Adv. Mater.*, 2009, **21**, 4087–4108.
- 15 Q. F. Zhang and G. Z. Cao, *Nano Today*, 2011, **6**, 91–109.
- 16 S. So, I. Hwang and P. Schmuki, *Energy Environ. Sci.*, 2015, **8**, 849–854.
- 17 J. Dou, Y. F. Li, F. Y. Xie, X. K. Ding and M. D. Wei, *Cryst. Growth Des.*, 2016, **16**, 121–125.
- 18 Z. Q. Li, Y. P. Que, L. E. Mo, W. C. Chen, Y. Ding, Y. M. Ma, L. Jiang, L. H. Huand and S. Y. Dai, *ACS Appl. Mater. Interfaces*, 2015, **7**, 10928–10934.



19 Y. J. Xiong, H. G. Cai, B. J. Wiley, J. G. Wang, M. J. Kim and Y. N. Xia, *J. Am. Chem. Soc.*, 2007, **129**, 3665–3675.

20 T. Oekermann, T. Yoshida, H. Minoura, K. G. U. Wijayantha and L. M. Peter, *J. Phys. Chem. B*, 2004, **108**, 8364–8370.

21 K. Zhu, N. R. Neale, A. Miedaner and A. J. Frank, *Nano Lett.*, 2007, **7**, 69–74.

22 T. Oekermann, D. Zhang, T. Yoshida and H. Minoura, *J. Phys. Chem. B*, 2004, **108**, 2227–2235.

23 H. J. Snaith and C. Ducati, *Nano Lett.*, 2010, **10**, 1259–1265.

